PROPERTIES OF PARTIALLY STABILIZED ZIRCONIA COMPONENTS FABRICATED BY THE CERAMIC ON-DEMAND EXTRUSION PROCESS

Wenbin Li[1], Amir Ghazanfari[1], Devin McMillen[1], Ming C. Leu[1], Gregory E. Hilmas[2]
and Jeremy Watts[2]

[1]Department of Mechanical and Aerospace Engineering, Missouri University of Science and
Technology, Rolla, MO, USA
[2]Department of Materials Science and Engineering, Missouri University of Science and
Technology, Rolla, MO, USA

Abstract

The Ceramic On-Demand Extrusion (CODE) process is a novel additive manufacturing process for fabricating dense ceramic components from aqueous pastes of high solids loading. In this study, 3 mol% Y_2O_3 stabilized tetragonal zirconia polycrystal (3Y-TZP) parts were fabricated using the CODE process. The parts were then dried in a humidity controlled environmental chamber and sintered under atmospheric pressure. Mechanical properties of the sintered parts were examined using ASTM standard test techniques, including density, Young's modulus, flexural strength, Weibull modulus, fracture toughness and Vickers hardness. The microstructure was analyzed, and grain size was measured using scanning electron microscopy. The results compared with those from Direct Inkjet Printing, Selective Laser Sintering, and other extrusion-based processes indicated that zirconia parts produced by CODE exhibit superior mechanical properties among the additive manufacturing processes. Several example parts were produced to demonstrate CODE's capability for fabricating geometrically complex ceramic parts.

Introduction

The Ceramic On-Demand Extrusion (CODE) is a novel extrusion-based additive manufacturing (AM) process, which produces dense ceramic components after sintering. It deposits high solids loading (>50 vol%) aqueous ceramic pastes onto a substrate layer-by-layer at room temperature. Each deposited layer is solidified by uniform infrared radiation drying from the top. At the same time, the undesirable water evaporation from the side of the part is prohibited by surrounding the part with liquid [1]. This layered uniform radiation drying approach eliminates the water content gradient in the fabricated part and thus enables the CODE process to produce crack-free ceramic parts. The progressive cavity pump based extruder utilized in CODE guarantees a precise Extrusion-On-Demand (EOD) control as well as a consistent deposition flowrate to avoid pores in the part [2], which further improves the density of the as-printed part.

Zirconia ceramics, especially 3Y-TZP (3 mol% Y_2O_3 stabilized tetragonal zirconia polycrystal), are important structural ceramic materials due to the superior mechanical properties resulting from the transformation toughening mechanism [3]. Additive manufacturing provides the capability of producing components with high geometrical complexity. However, most ceramic additive manufacturing processes exhibit less than satisfactory mechanical properties

due to residual porosity in the final products, a result of additive manufacturing processes, and the flaw-sensitive nature of ceramic materials. Thus, pursuing high mechanical properties is a challenge of ceramic additive manufacturing. In the work described in the present paper, the CODE process was used to fabricate 3Y-TZP specimens and their mechanical properties and resulting microstructure were evaluated.

Experimental procedure

Paste preparation

A commercially available zirconium oxide powder (TZ-3Y-E, Tosoh USA, Inc., Grove City, OH, USA) was selected as the raw material. Characteristics of the raw powder provided by the manufacturer are summarized in Table 1. Batches of ceramic suspensions (paste) were produced in 100 mL quantities and consisted of 50 vol% ceramic solids using distilled water, 30% ammonia ammonium hydroxide solution (NH_4OH Sigma Aldrich, St. Louis, MO, USA), and 5 wt% Dolapix CE 64 (R-C(O)OH, Zschimmer & Schwarz, Inc., Lahnstein, Rhineland-Palatinate, Germany) dispersant. The suspensions were mixed within 24 hours prior to part fabrication. The pH was adjusted drop-wise using the ammonium hydroxide solution until alkaline pH $\approx$ 9-10 was achieved, as measured by a pH meter (HI 2210, Hannah Instruments, Woonsocket, RI, USA). Prior dispersion studies confirmed suspension stability in the alkaline pH range. The solids were added slowly and stirred. All mixing was done using a vacuum power whip mixer (Model F, Whip Mix, Louisville, KY, USA), pulling a mild vacuum (~20 kPa) during discrete mixing steps to aid in deaeration, until all solids were added. The paste was then stirred for five minutes under vacuum to homogenize and agitated on a vibratory table to remove entrapped air.

Table 1. Characteristics of ZrO_2 powder (data provided by Tosoh USA, Inc.).

Powder Grade	TZ-3Y-E
Surface Area (m^2/g)	16 ± 3
Actual Particle Size (μm)	0.04
Y_2O_3 Content (mol%)	3
Impurity Level (wt%)	5.2 ± 0.5 Y_2O_3
	< 5.0 HfO_2
	0.1-0.4 Al_2O_3
	≤ 0.02 SiO_2
	≤ 0.01 Fe_2O_3
	≤ 0.04 Na_2O

Part building process

The zirconia paste was extruded at controlled flowrates through a circular nozzle. While the nozzle moved under the control of G&M codes, the extruded material was deposited on a substrate located in a tank designed to hold a fluid medium. Once the deposition of each layer

was completed, oil was pumped into the tank surrounding the layer to prevent undesirable water evaporation from the sides of the deposited layers. A mineral oil (Florasense Lamp Oil, MVP Group International Inc., Charleston, SC, USA) was chosen as the fluid surrounding the part to preclude interaction between the fluid and the paste. The level of oil was controlled so that it was maintained at a level just below the top surface of the part being fabricated. Infrared radiation was then applied to uniformly dry the deposited layer from the top, so that the part being fabricated would maintain its shape while proceeding layers were deposited. By repeating the above steps, the part was fabricated layer-by-layer. A schematic of the process is shown in Figure 1. The layered, uniform radiation drying, together with the prohibition of undesirable evaporation from the sides of the part, enable rapid solidification of each layer without causing moisture gradients in the part, thus preventing cracking and warpage. The remaining water content was eliminated in the post processing.
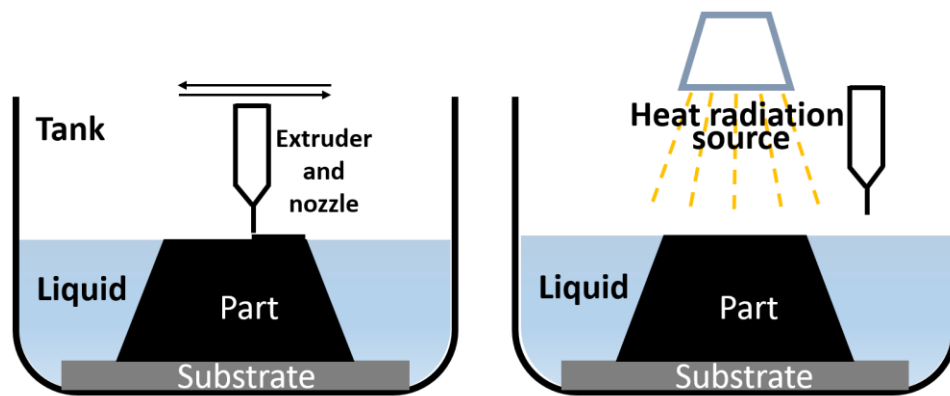

Figure 1. Schematic of part building process of CODE.

In this study, 24 beams with dimensions of 6 mm × 25 mm × 4 mm (width × length × depth, in CAD model), and 5 blocks with dimensions of 53.2 mm × 53.2 mm × 6.4 mm (width × length × depth, in CAD model) were printed for property evaluation.

Post processing

Once the parts were built and removed from the tank, the remaining water content in the parts and the oil on the surface of the parts were eliminated by bulk-drying to obtain "green" parts. The bulk-drying was performed in an environmental chamber where the relative humidity and temperature were controlled to 75% and 25 °C for 20 hours. The high humidity in the chamber slowed down the drying rate to avoid warpage and crack formation. The green parts were then sintered in an electric furnace under atmospheric pressure to obtain the final parts.

In order to determine the right sintering temperature vs. time, a sintering study was performed on the zirconia beams. The 24 "green" beams were divided in to 8 groups, and sintered under 8 different sintering conditions. The 8 groups of sintered specimens were then tested to compare their density, hardness and fracture toughness. The best sintering condition among the 8 groups was determined through comparison. The 5 "green" zirconia blocks were then sintered under this selected condition. Figure 2 shows one of the 5 sintered blocks. The printing parameters for all specimens are also listed in this figure.
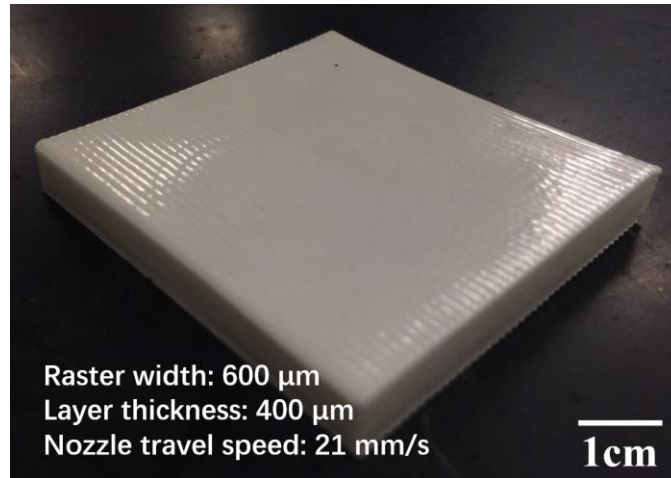
Figure 2. A sintered 3Y-TZP block fabricated by the CODE process.

Property evaluation

Density of sintered parts were determined by Archimedes' method [4]. The dry mass of each specimen was measured first. Then, the specimens were saturated by submersion in distilled water and placing them under vacuum for 12 h. The saturated and suspended masses were then recorded to calculate the final density.

Vickers hardness was obtained according to ASTM C1327 [5] with a hardness tester (V-100-V2, LECO, Saint Joseph, MI, USA). The applied force was 98.07 N for 10 seconds. The test surfaces of specimens were polished using successively finer diamond abrasives down to 0.25 μm prior to indentation.

For the 24 sintered beams, fracture toughness was estimated from the indentation test due to its simplicity using Anstis' method [6]. For the blocks sintered at the selected final sintering condition, fracture toughness was measured by the Chevron-Notched (CN) beam method according to ASTM C1421 [7] using an instrumented load frame (Instron 5881, Instron corporation, Norwood, MA, USA), and a crosshead velocity of 0.2 mm/min.

Flexural strength was measured by the four-point bending method (Instron 5881, Instron corporation, Norwood, MA, USA) according to ASTM C1161 [8]. The Young's modulus was determined using a deflectometer (a linear variable differential transformer) measuring the deflection of the center of the test beam during the bending test. Both A-size (2mm × 1.5mm × 25mm) and B-size (4mm × 3mm × 45mm) beam specimens were prepared and tested. From the 5 sintered blocks, 30 A-size specimens and 30 B-size specimens were cut. All four surfaces of each specimen were ground by a 600-grit diamond wheel.

The specimen's microstructure was examined by scanning electron microscopy (SEM) (Helios Nanolab 600, FEI, OR, USA). Prior to SEM imaging, the specimen was first polished down to 0.25 micron using successively finer abrasive diamond particles, then thermally etched at 1350 °C for 0.5 hour. The average grain size was measured by an image processing method using ImageJ, an open-source image processing software.

Results and discussion

Study of sintering conditions

There were 24 beam specimens (6 mm × 25 mm × 4 mm, in CAD model) studied. They were divided into 8 groups, each group having 3 specimens, and sintered at 8 different sintering conditions, i.e. different temperatures (T) and hold times (t). The relative density (D) and Vickers hardness (HV) were measured, and the fracture toughness (K_{IC}) was estimated from the indentation test for each group of specimens. The theoretical density (T.D.) of 3Y-TZP is 6.10 g/cm^3 [9][10][11]. The bulk density of each group was measured from 3 specimens. The hardness was measured from 6 indentations on 3 specimens. The fracture toughness was then calculated according to Equation (1) from the 6 indentations on 3 specimens.

$$K_{IC} = \S(E/H)^{1/2} P/c^{3/2} \tag{1}$$

where $\S$ is a constant (0.016) [12][13], H is the hardness (GPa), P is the applied load (N), E is the Young's modulus (GPa), and c is the crack half-length (m), which is the diagonal length of the indent plus the two crack lengths, divided by 2 (see Figure 3). The elastic modulus used in Equation (1) was 210 GPa, which is a commonly used value in most of the fracture toughness test of 3Y-TZP [10][11][12]. The applied load was 98.07 N. The average results as well as the standard deviation are given in Table 2.
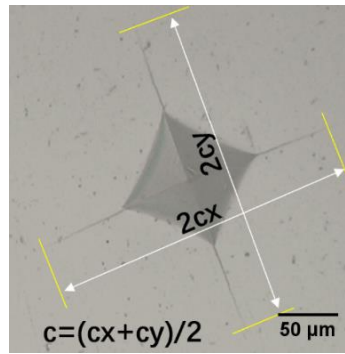

Figure 3. Micrograph of a Vickers indent and cracks.

Table 2. Density, hardness and fracture toughness results of the 8 sintering groups.

	T (°C)	t (h)	D (%)	HV (GPa)	K_{Ic} (MPa.m$^{0.5}$)
Group 1	1350	1	98.40 (0.31)	14.2 (0.19)	3.5 (0.04)
Group 2	1350	2	98.81 (0.01)	14.1 (0.09)	3.5 (0.05)
Group 3	1450	0.5	98.76 (0.07)	13.9 (0.21)	3.7 (0.09)
Group 4	1450	1	98.61 (0.13)	13.7 (0.16)	3.8 (0.07)
Group 5	1500	0.5	98.51 (0.22)	13.8 (0.24)	3.8 (0.14)
Group 6	1500	1	98.41 (0.12)	13.8 (0.12)	3.7 (0.06)
Group 7	1550	0.5	98.38 (0.04)	13.4 (0.35)	4.0 (0.07)
Group 8	1550	1	98.44 (0.09)	13.1 (0.14)	4.3 (0.08)

Note: Values in parentheses show the standard deviation.

According to Table 2, all groups had a density above 98% of theoretical density; and group 2 (1350°C, 2h) reached a maximum density of 98.8%, while group 8 (1550 °C, 1 h) had the highest fracture toughness (4.3 MPa•m$^{0.5}$). Although it exhibited the lowest hardness, the sintering condition of group 8 was determined to be the best among all groups since it resulted in the highest fracture toughness, which is more desirable for 3Y-TZP than hardness.

Shrinkage

There were 5 blocks (53.2 mm × 53.2 mm × 6.4 mm, in CAD model) sintered at the selected sintering condition (1550 °C, 1 h). Their final dimensions were measured by a Vernier caliper after sintering. An isotropic linear shrinkage of ~20% was observed, as given in Table 3.

Table 3. Dimensions of sintered specimens and shrinkage in different directions.

	Width	Length	Depth	Shrinkage (%)		
	(mm)	(mm)	(mm)	Width	Length	Depth
#1	42.43	42.44	5.02	20.2	20.2	21.6
#2	42.44	42.58	5.01	20.2	20.0	21.7
#3	42.43	42.58	5.04	20.2	20.0	21.3
#4	42.44	42.54	5.01	20.2	20.0	21.7
#5	42.30	42.39	5.02	20.5	20.3	21.6
Average				20.3	20.1	21.6

Fracture toughness

Chevron-Notched (CN) beams were prepared from 16 B-size beams, out of which 8 CN beams were successfully cut, the other 8 were disposed due to large cutting errors. For the 8 CN beams, the first 2 tests failed to give stable load curves, so a simple compression-compression fatiguing procedure was applied to the other 6 specimens according to ASTM C1421 [7]. After the compression-compression fatigue cycle, all 6 specimens had stable crack growth. The average fracture toughness (K_{Ivb}) was 4.6 MPa.m$^{0.5}$, with a standard deviation of 0.23 MPa.m$^{0.5}$.

Flexural strength and Young's modulus

Four-point bending tests were performed on 30 A-size beam specimens, of which 29 tests were valid. The mean flexural strength ($\bar{\sigma}_{A4}$) measured was 616 MPa, standard deviation was 87 MPa, and the maximum and minimum strengths were 754 MPa and 416 MPa. Young's modulus measured was 221 GPa, with a standard deviation of 12.3 GPa, which is close to the assumed value used in Equation (1).

The Weibull distribution parameters of the flexural strength values of the above 29 specimens were estimated according to ASTM C1239 [14]. The Weibull plot is shown in Figure 4. A regression analysis was performed using Matlab to estimate the Weibull modulus, $\hat{m}$ (the slope of the fitted line). From the regression analysis, $\hat{m} = 8.3$ was obtained. However, the estimated Weibull modulus ($\hat{m}$) generally exhibits statistical bias. The amount of statistical bias depends on the number of test specimens. An unbiased estimate of m can be obtained by

multiplying $\hat{m}$ by an unbiasing factor provided in ASTM C1239. For 29 specimens, an unbiasing factor of 0.951 was used, resulting in the unbiased estimate of Weibull modulus of $m = 7.9$.
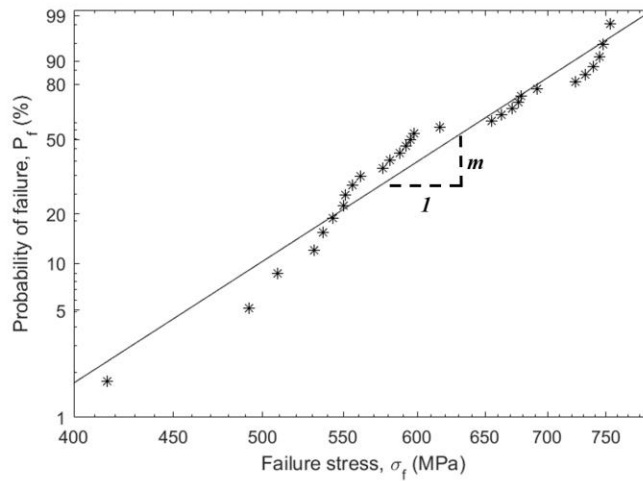

Figure 4. Weibull plot for 29 A-size beam specimens.

Among the 30 B-size beam specimens, 16 were used for preparing Chevron-Notched beams for the fracture toughness test, 4 were damaged during machining. For the remaining 10, their flexural strengths were also measured through four-point bending tests, revealing a mean flexural strength ($\bar{\sigma}_{B4}$) of 563 MPa.

Microstructure

An SEM micrograph showing the general microstructure of a sintered 3Y-TZP specimen is shown in Figure 5. Excluding the grains at the edges of the image, a total number of 419 complete grains were counted in the micrograph. The area of each grain was recorded using ImageJ. By assuming a circular shape for each grain, their diameters were calculated. The average area of grains was 0.26 μm^2, with a standard deviation of 0.22 μm^2. The average ZrO_2 grain size, reported as the average diameter. was 0.52 μm, with a standard deviation of 0.24 μm.
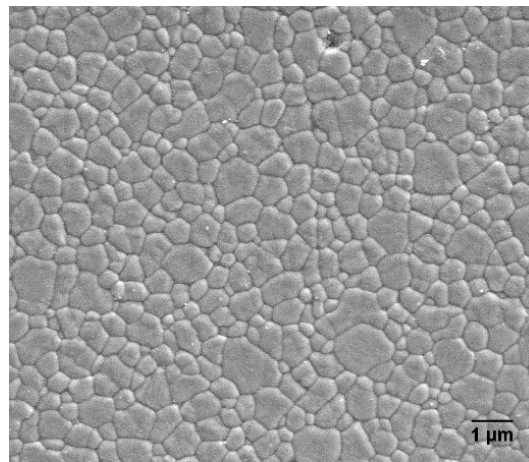

Figure 5. SEM micrograph showing the microstructure of specimens sintered at 1550 °C for 1 h.

Comparison to other processes

In order to evaluate the relative quality of CODE fabricated 3Y-TZP parts, a property comparison to conventional ceramic fabrication processes and ceramic additive manufacturing processes was made. Among various conventional processes, some sinter the green part under high pressure, such as hot pressing and hot isostatic pressing. The pressurized sintering process increases the strength of the final part considerably [15]. In order to have a fair comparison, only processes which sinter at atmospheric pressure were considered to compare. In addition, the raw material may also affect the properties of the final part. By considering those effects, the property data provided by the powder manufacturer (Tosoh USA Inc., Grove city, OH, USA) was used for comparison. According to the datasheet, their specimens were first shaped by cold pressing under 70 MPa uniaxial pressure for 30 seconds, then sintered at atmospheric pressure. From the properties provided by the powder manufacturer, the three-point bending flexural strength for the TZ-3Y-E powder is $\bar{\sigma}_{3YB3} = 1000\ MPa$, and $\bar{\sigma}_{3YSB3} = 1500\ MPa$ for the TZ-3YS-E powder [4].

Several additive manufacturing processes have been developed for ceramics, including Stereolithography (SLA) [16], Lithography-based Ceramic Manufacturing (LCM) [17], Robocasting [18], Fused Deposition of Ceramics (FDC) [19], Freeze-Form Extrusion (FFE) [20], Selective Laser Sintering (SLS) [21][22], Selective Laser Melting (SLM) [23], Thermoplastic 3D-Printing (T3DP) [24], Direct Inkjet Printing (DIP) [25] and Extrusion-based Photo-initiate Polymerization [26]. Among them, a number of attempts to fabricate zirconia parts have been made in the past 20 years.

Bertrand et al. [21] and Shahzad et al. [22] employed SLS to fabricate zirconia parts. Bertrand et al. directly sintered the pure Y_2O_3-ZrO_2 powder to obtain the final part. The density of their as-fabricated part was 56% of theoretical density (T.D.), and they also reported that further sintering in a conventional furnace cannot increase the density. Shahzad et al. prepared a powder mixture containing Y_2O_3-ZrO_2 powder and isotactic polypropylene (PP). They used SLS to melt the sacrificial organic binder (PP) phase to produce green parts and sintered the green part to obtain the final part. The density of their sintered 3Y-TZP parts was only 32% of T.D.; however, they reported that the combination of pressure infiltration (PI) of ZrO_2 suspension and warm isostatic pressing (WIP) could increase the final density to 85% of T. D.

Scheithauer et al. [24] developed the Thermoplastic 3D Printing process which combines FDM and robocasting. They used thermoplastic binder systems and Y_2O_3-ZrO_2 powder to prepare highly loaded feedstocks that were processed in a heated dispensing unit. The density of their sintered 3Y-TZP parts was reported to be 98% of T. D. and only single-wall specimens were produced.

Faes et al. [26] prepared a dispersion based on ceramic powders and UV-resin. The dispersion is selectively deposited through a nozzle while being cured by an LED array. This process was referred to as extrusion-based AM using photo-initiated polymerization. The density reported for their sintered 3Y-TZP parts was 92% of T. D.

Özkol et al. [25] applied the direct inkjet printing (DIP) process to fabricate 3Y-TZP parts. They prepared aqueous ink containing 40 vol% of Y_2O_3–ZrO_2 particles and used a

modified HP office-type thermal inkjet printer to print the ink. The printed parts were then dried and sintered. An absolute density of 5.82 g/cm^3 was reported, which corresponds to 95.4% of T. D. They also reported the Weibull characteristic flexural strength ($\sigma_{\theta DIP}$), mean flexural strength ($\bar{\sigma}_{DIP}$) and Weibull modulus (m_{DIP}), which were 843 MPa, 759 MPa and 3.6, respectively.

A direct comparison can be made for properties including density (*D*), hardness (*H*), fracture toughness (K_{IC}), and Weibull modulus (*m*). However, the observed strength values of advanced ceramics are dependent on the test specimen size, geometry and stress state. Prior to making flexural strength comparisons, conversions are needed to account for the different specimen sizes and test configurations.

ASTM C1683 [27] standard provides a methodology to convert the mean flexural strengths determined from different test configurations. According to [25], the flaw distribution was assumed to be volume-based, and Equation (2) was used to convert the four-point bending flexural strength value of DIP specimens under DIP configuration ($\bar{\sigma}_{DIP}$) to the four-point bending flexural strength value under ASTM B-size configuration ($\bar{\sigma}_{DIPB4}$). Equation (3) was then used to convert $\bar{\sigma}_{DIPB4}$ to the three-point bending flexural strength value under Tosoh's configuration ($\bar{\sigma}_{DIPB3}$).

$$(\sigma_0)_v = \frac{\bar{\sigma}_{B4}\left\{\left[\left(\dfrac{L_{i4}}{L_{o4}}\right)\cdot m+1\right]\cdot\left[\dfrac{1}{2(m+1)^2}\right]\cdot b\cdot d\cdot L_{o4}\right\}^{1/m}}{\Gamma\left(\dfrac{1}{m}+1\right)} \tag{2}$$

$$\frac{\bar{\sigma}_{B3}}{\bar{\sigma}_{B4}}=\left(\frac{L_{o4}}{L_{o3}}\right)^{1/m}\left(\frac{m+2}{2}\right)^{1/m} \tag{3}$$

Also, the flexural strength of CODE specimens under ASTM B-size configuration ($\bar{\sigma}_{CODEB4}$) was converted to obtain three-point bending flexural strength values which would correspond to the Tosoh's configuration ($\bar{\sigma}_{CODEB3}$) using Equation (3), irrespective of whether the flaws are surface- or volume-distributed. The nomenclature for Equations (2) and (3) is given below:

$\bar{\sigma}_{B4}$ = mean strength for a four-point flexure test specimen;
$\bar{\sigma}_{B3}$ = mean strength for a three-point flexure test specimen;
m = Weibull modulus;
b = width of a flexure test specimen;
d = thickness of a flexure test specimen;
L_{i4} = length of the inner span for a four-point flexure test specimen;
L_{o4} = length of the outer span for a four-point flexure test specimen;
L_{o3} = length of the outer span for a three-point flexure test specimen;

The final converted results were $\bar{\sigma}_{CODEB3} = 712$ MPa and $\bar{\sigma}_{DIPB3} = 723$ MPa, which can be directly compared with the strength value provided by Tosoh (i.e. $\bar{\sigma}_{3YB3}$ and $\bar{\sigma}_{3YSB3}$). $\bar{\sigma}_{CODEB3}$ was compared to $\bar{\sigma}_{3YB3}$ since TZ-3Y-E powder was used in the CODE process, while $\bar{\sigma}_{DIPB3}$ was compared to $\bar{\sigma}_{3YSB3}$, which corresponds to the TZ-3YS-E powder used.

Table 4 summarizes the mechanical properties comparison made between the CODE process, a representative conventional ceramic fabrication process, and other AM processes. The density (D) values in Table 4 are the highest values found in the literature. It can be seen from this table that the CODE fabricated parts have the highest density among all AM processes. Their flexural strength reaches ~70% of that of cold uniaxial pressed parts, and their hardness and fracture toughness are close to that of cold uniaxial pressed parts. The non-disclosed properties are marked as "N.D.".

Table 4. Mechanical properties from different ZrO2 ceramic fabrication processes.

		Raw powder	*D* (%)	*H* (GPa)	K_{Ic} (MPam$^{0.5}$)	σ (MPa)	*m*	**Comments**
Conventional	Cold uniaxial pressing	TZ-3Y-E[1]	99.2	12.3	5	1000	N.D	Provided by Tosoh
		TZ-3YS-E[1]	99.2	12.3	5	1500	N.D	
AM	SLS [21] [22]	ZYP30[2]	56.0	N.D.	N.D.	N.D.	N.D	--
	T3DP[3] [24]	TZ-3YS-E	98.0	N.D.	N.D.	N.D.	N.D	--
	EPP[4] [26]	TZ-3Y-E	92.0	N.D.	N.D.	N.D.	N.D	--
	DIP [25]	TZ-3YS-E	95.4	N.D.	N.D.	723	3.6	48.2% of $\bar{\sigma}_{3YSB3}$
	CODE	TZ-3Y-E	98.4	13.1	4.6	715	7.9	71.5% of $\bar{\sigma}_{3YB3}$

Note: 1. Tosoh USA, Inc., Grove City, OH, USA
2. Zircar Zirconia, Inc., Florida, NY, USA
3. Thermoplastic 3D Printing
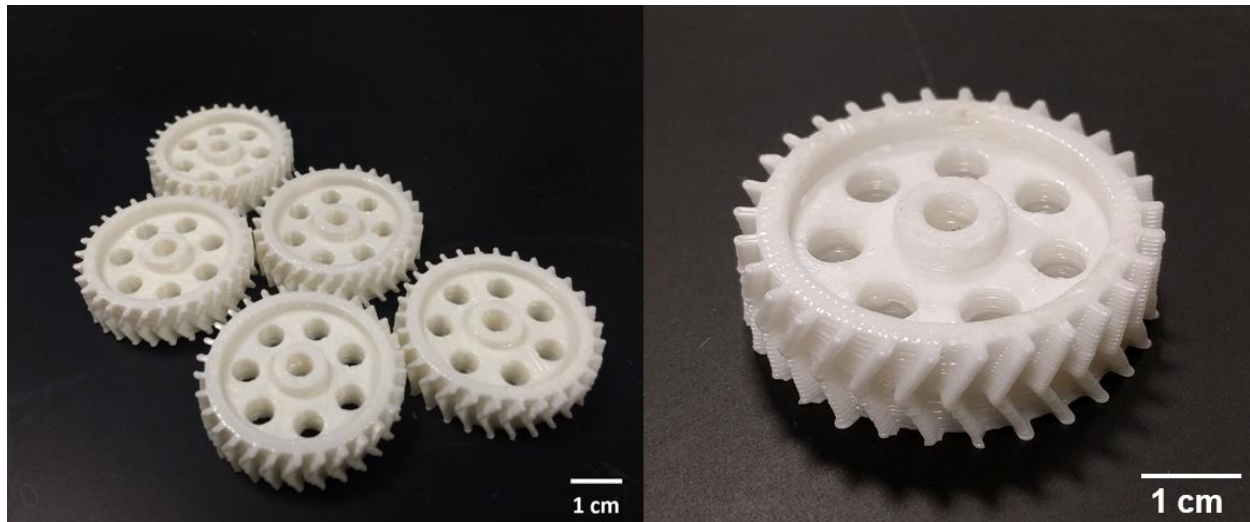4. Extrusion-based AM using photo-initiated polymerization

Figure 6. Five double helical gears (sintered) fabricated by using the CODE process and close-up view of one gear.

Example parts

To demonstrate the capabilities of the CODE process to fabricate 3D parts with complex geometries and validate the printability of the ZrO_2 paste, several double helical 3Y-TZP gears were successfully fabricated and sintered. As shown in Figure 6, the parts were free of pores between contours and infill lines.

Conclusions

An aqueous paste consisting of 3 mol% yttria-stabilized zirconia was developed and the Ceramic On-Demand Extrusion (CODE) process was employed to fabricate 3Y-TZP test specimens and example parts. The properties of fabricated test specimens were examined. A maximum relative density of 98.8% was achieved. The Vickers hardness (HV) and fracture toughness (K_{Ivb}) measured were 13.1 GPa and 4.6 MPa.m$^{0.5}$, respectively. The flexural strength obtained from a four-point bending test (ASTM C1161 A-size configuration) was 616 MPa, from which the estimated three-point bending strength was 715 MPa.

The measured results were compared to other AM processes and a representative conventional process. This comparison reveals that the CODE fabricated parts have the highest density among all AM processes. Their flexural strength reached ~70% of that of cold uniaxial pressed parts, and the hardness and fracture toughness were close to that of cold uniaxial pressed parts. Several double helical 3Y-TZP gears were successfully fabricated, which demonstrated CODE's capability of fabricating non-sparse parts having a complex geometry.

Acknowledgements

References

[1] Ghazanfari, A., W. Li, M.C. Leu, and G.E. Hilmas. "A Novel Extrusion-based Additive Manufacturing Process for Ceramic Parts." Paper presented at the *Solid Freeform Fabrication Symposium*, *Austin, TX,* 2016.

[2] Li, W., A. Ghazanfari, M.C. Leu, and R.G. Landers. "Methods of extrusion on demand for high solids loading ceramic paste in freeform extrusion fabrication." Paper presented at the *Solid Freeform Fabrication Symposium, Austin, TX,* 2015.

[3] Hannink, R., H.J. Hannink, P.M. Kelly, and B.C. Muddle. "Transformation toughening in zirconia‐containing ceramics." *Journal of the American Ceramic Society* 83, no. 3 (2000): 461-487. doi: 10.1111/j.1151-2916.2000.tb01221.x

[4] Tosoh*, Tosoh zirconia powder specification and typical properties*. Tosoh Corpration, Tokyo, Japan, 2003.

[5] ASTM International. *ASTM C1327-15 Standard Test Method for Vickers Indentation Hardness of Advanced Ceramics*. West Conshohocken, PA: ASTM International, 2015. doi:

10.1520/C1327-15.

[6]   Anstis, G.R., P. Chantikul, B.R. Lawn, and D.B. Marshall. "A critical evaluation of indentation techniques for measuring fracture toughness: I, direct crack measurements." *Journal of the American Ceramic Society* 64, no. 9 (1981): 533-538. doi: 10.1111/j.1151-2916.1981.tb10320.x

[7]   ASTM International. *ASTM C1421-16 Standard Test Methods for Determination of Fracture Toughness of Advanced Ceramics at Ambient Temperature*. West Conshohocken, PA: ASTM International, 2016. doi: 10.1520/C1421-16.

[8]   ASTM International. *ASTM C1161-13 Standard Test Method for Flexural Strength of Advanced Ceramics at Ambient Temperature*. West Conshohocken, PA: ASTM International, 2013. doi: 10.1520/C1161.

[9]   Ghatee, M., M.H. Shariat, and J.T.S. Irvine. "Investigation of electrical and mechanical properties of 3YSZ/8YSZ composite electrolytes." *Solid State Ionics* 180, no. 1 (2009): 57-62. doi: 10.1016/j.ssi.2008.10.006

[10]   Trunec, M. "Effect of grain size on mechanical properties of 3Y-TZP ceramics." *Ceramics Silik* 52, no. 3 (2008): 165-171. doi: 10.1111/j.1551-2916.2007.01643.x

[11]   Trunec, M., and Z. Chlup. "Higher fracture toughness of tetragonal zirconia ceramics through nanocrystalline structure." *Scripta Materialia* 61, no. 1 (2009): 56-59. doi: 10.1016/j.scriptamat.2009.03.019

[12]   Cottom, B.A., and M.J. Mayo. "Fracture toughness of nanocrystalline ZrO_2-3mol% Y_2O_3 determined by Vickers indentation." *Scripta materialia* 34, no. 5 (1996): 809-814. doi: 10.1016/1359-6462(95)00587-0

[13]   Kosmač, T., C. Oblak, P. Jevnikar, N. Funduk, and L. Marion. "The effect of surface grinding and sandblasting on flexural strength and reliability of Y-TZP zirconia ceramic." *Dental Materials* 15, no. 6 (1999): 426-433. doi: 10.1016/S0109-5641(99)00070-6

[14]   ASTM International. *ASTM C1239-13 Standard Practice for Reporting Uniaxial Strength Data and Estimating Weibull Distribution Parameters for Advanced Ceramics*. West Conshohocken, PA: ASTM International, 2013. doi: 10.1520/C1239.

[15]   Guazzato, M., M. Albakry, S.P. Ringer, and M.V. Swain. "Strength, fracture toughness and microstructure of a selection of all-ceramic materials. Part II. Zirconia-based dental ceramics." *Dental materials* 20, no. 5 (2004): 449-456. doi: 10.1016/j.dental.2003.05.002

[16]   Chartier, T., C. Chaput, F. Doreau, and M. Loiseau. "Stereolithography of structural complex ceramic parts." Journal of Materials Science 37, no. 15 (2002): 3141-3147. doi: 10.1023/A:1016102210277

[17]   Schwentenwein, M., and J. Homa. "Additive manufacturing of dense alumina ceramics." *International Journal of Applied Ceramic Technology* 12, no. 1 (2015): 1-7. doi: 10.1111/ijac.12319

[18]   Travitzky, N., A. Bonet, B. Dermeik, T. Fey, I. F. Demut, L. Schlier, T. Schlordt, and P. Greil. "Additive Manufacturing of Ceramic‐Based Materials." *Advanced Engineering Materials* 16, no. 6 (2014): 729-754. doi: 10.1002/adem.201400097

[19] Agarwala, M.K., R.V. Weeren, A. Bandyopadhyay, P.J. Whalen, A. Safari, and S.C. Danforth. "Fused deposition of ceramics and metals: an overview." Paper presented at the *Solid Freeform Fabrication Symposium, Austin, Texas*. 1996.

[20] Huang, T., M.S. Mason, G.E. Hilmas, and M.C. Leu. "Freeze-form extrusion fabrication of ceramic parts." *Virtual and Physical Prototyping* 1, no. 2 (2006): 93-100.doi: 10.1080/17452750600649609

[21] Bertrand, P., F. Bayle, C. Combe, P. Goeuriot, and I. Smurov. "Ceramic components manufacturing by selective laser sintering." *Applied Surface Science* 254, no. 4 (2007): 989-992. doi: 10.1016/j.apsusc.2007.08.085

[22] Shahzad, K., J. Deckers, Z. Zhang, J.P. Kruth, and J. Vleugels. "Additive manufacturing of zirconia parts by indirect selective laser sintering." *Journal of the European Ceramic Society* 34, no. 1 (2014): 81-89. doi: 10.1016/j.jeurceramsoc.2013.07.023

[23] Wilkes, J., Y.C. Hagedorn, W. Meiners, and K. Wissenbach. "Additive manufacturing of ZrO_2-Al_2O_3 ceramic components by selective laser melting." *Rapid Prototyping Journal* 19, no. 1 (2013): 51-57. doi: 10.1108/13552541311292736

[24] Scheithauer, U., E. Schwarzer, H.J. Richter, and T. Moritz. "Thermoplastic 3D printing—an additive manufacturing method for producing dense ceramics." *International Journal of Applied Ceramic Technology* 12, no. 1 (2015): 26-31. doi: 10.1111/ijac.12306

[25] Özkol, E., W. Zhang, J. Ebert, and R. Telle. "Potentials of the "Direct inkjet printing" method for manufacturing 3Y-TZP based dental restorations." *Journal of the European Ceramic Society* 32, no. 10 (2012): 2193-2201. doi: 10.1111/ijac.12306

[26] Faes, M., J. Vleugels, F. Voguer, and E. Ferraris. "Extrusion-based additive manufacturing of ZrO_2 using photoinitiated polymerization." *CIRP Journal of Manufacturing Science and Technology* (2016). doi: 10.1016/j.cirpj.2016.05.002

[27] ASTM International. *ASTM C1683-10(2015) Standard Practice for Size Scaling of Tensile Strengths Using Weibull Statistics for Advanced Ceramics*. West Conshohocken, PA: ASTM International, 2015. doi: 10.1520/C1683-10R15